DYNA Ingeniería e Industria	STUDY OF FLUID DYNAMICS AND SULFUR MASS TRANSFER BETWEEN STEEL AND SLAG IN A LADLE FURNACE CONSIDERING DRAG AND NON-DRAG FORCES	1203 COMPUTER SCIENCE
RESEARCH ARTICLE	Antonio Urióstegui-Hernández, Pedro Garnica-González, Constantin-Alberto Hernández-Bocanegra, José-Ángel Ramos-Banderas, José-Julián Montes-Rodríguez, José-Raúl Ortiz-Castillo.	1203.26 Simulation

STUDY OF FLUID DYNAMICS AND SULFUR MASS TRANSFER BETWEEN STEEL AND SLAG IN A LADLE FURNACE CONSIDERING DRAG AND NON-DRAG FORCES

ESTUDIO DE LA DINÁMICA DE FLUIDOS Y LA TRANSFERENCIA MÁSICA DE AZUFRE ENTRE EL ACERO Y LA ESCORIA EN UN HORNO OLLA CONSIDERANDO FUERZAS DE ARRASTRE Y NO-ARRASTRE

Antonio Urióstegui-Hernández, Pedro Garnica-González, Constantin-Alberto Hernández-Bocanegra, José-Ángel Ramos-Banderas, José-Julián Montes-Rodríguez y José-Raúl Ortiz-Castillo

Tecnológico Nacional de México. Instituto Tecnológico de Morelia. Av. Tecnológico #1500 – 58120 Morelia (México)

Received: 03/may/2021 • Reviewing: 06/may/2021 • Accepted 21/sep/2021 DOI: https://doi.org/10.6036/10206

TO CITE THIS ARTICLE:

URIÓSTEGUI-HERNÁNDEZ, Antonio; GARNICA-GONZÁLEZ, Pedro; HERNÁNDEZ-BOCANEGRA, Constantin-Alberto; RAMOS-BANDERAS, José-Ángel; MONTES-RODRÍGUEZ, José-Julián; ORTIZ-CASTILLO, José-Raúl. STUDY OF FLUID DYNAMICS AND SULFUR MASS TRANSFER BETWEEN STEEL AND SLAG IN A LADLE FURNACE CONSIDERING DRAG AND NON-DRAG FORCES. Dyna March-April 2022. Vol. 97 no. 2 . DOI: https://doi.org/10.6036/10206

ABSTRACT:

In this work fluid dynamics and a basic study of the sulfur transfer at the steel/slag interface in the ladle during argon gas agitation was developed. Mass transfer and chemical reaction models coupled with Computational Fluid Dynamics (CFD) were employed. The multiphasic simulation was solved using the Eulerian model considering drag and non-drag forces, and the flow pattern was validated through Particle Image Velocimetry (PIV) technique. The sulfur transfer rate was tracked by two approximations: (1) unidirectional constant rate Mass Transfer Model (MTM), and (2) unidirectional constant rate Mass Transfer Model coupled with Chemical Reaction Model (MTM+CRM) using Arrhenius equation. It was found that including the non-drag forces affects the fluid dynamics structure. Otherwise, the desulfurization rates increase as the argon gas flow rate increases, finding that the MTM model predicts ~15% less sulfur in the steel than the MTM+CRM, whose results were compared with plant measurements reports.

Keywords: Simulation; mathematical model; secondary steelmaking

RESUMEN:

En este trabajo, se desarrolló un estudio básico de la dinámica de fluidos y la transferencia de azufre en la interface acero/escoria en un horno olla durante la agitación con gas argón. Se empleó la Dinámica de Fluidos Computacional (CFD) acoplada con los modelos de transferencia de masa y reacción química. La simulación multifásica fue resulta usando el modelo Euleriano, considerando las fuerzas de arrastre y no-arrastre, mientras que los patrones de flujo se validaron mediante la técnica de Velocimetría por Imágenes de Partículas (PIV). La tasa de transferencia de azufre se monitoreó a través de dos aproximaciones: (1) el Modelo de Transferencia de Masa constante unidireccional (MTM) y (2) el Modelo de Transferencia de Masa constante unidireccional acoplado con el Modelo de Reacción Química (MTM+CRM) que usa la ecuación de Arrhenius. Se encontró que la inclusión de las fuerzas de no-arrastre afecta la estructura de la dinámica de fluidos. Por otra parte, las velocidades de desulfuración se incrementan conforme el flujo de gas argón inyectado aumenta, encontrándose que el modelo MTM predice un ~15% menos azufre en el acero que el modelo MTM+CRM, y cuyos resultados fueron comparados con mediciones de planta.

Palabras clave: Simulación; modelo matemático; refinación secundaria.

1. INTRODUCTION

The secondary refining process is a set of operations that allows to improve the steel quality. In this process, the chemical and thermal adjustment of the steel are carried out as well as the cleaning control by the removal of nonmetallic inclusions. The reactor used for this purpose was the ladle which is essential in modern steelmaking processes; in this, a common operation that is carried out is the injection of an inert gas through a porous plug which locates at the bottom. The purpose of stirring the liquid steel is to improve the kinetics of the chemical reactions between the steel and the slag, as well as to obtain a bath more thermally homogeneous. The most important operation in this process is the sulfur removal from steel by synthetic slags, through various reaction mechanisms [1]. Sulfur

ISSN: 0012-7361 eISSN: 1989-1490 / DYNA March – April 2022 Vol.97 No 2 DOI: https://doi.org/10.6036/10206

is one of the most detrimental elements in steel, since it decreases their ductility and impact resistance [2,3]. Due to this, steel with an ultra-low sulfur content (<10 ppm) is increasingly demanded, which is used to produce high pressure pipes, marine platforms, automotive industry, bearings, etc. Normally, the desulfurization process consists of the conversion of sulfur to calcium sulfide (CaS) through the reaction with calcium oxide (CaO). Thus, secondary refining has been the object of several studies [4,5,6] to analyze the behavior of fluid dynamics and desulphurization; they have employed tools such as computer simulation programs and thermodynamic software. Some studies [7]-[9] have established models that allow to predict the mass transfer behavior and removal of sulfur in the ladle. However, these studies do not take into account the fluid dynamic behavior, which affect directly the results. Other studies [10]-[14] have aimed at observing the fluid dynamics behavior in the ladle, such as the formation and development of the gas plume, the opening of the slag layer, the mixing times and the fluid dynamics structure. However, these studies have left aside the chemical behavior, which is a fundamental part of the refining process. There have been attempts to couple fluid dynamics and chemical analysis in a single numerical simulation [15]-[19], for which it is required to have software compatible in each discipline which means an extra economic cost. Some works [20]-[22] have left out this coupling, using the programming of some functions and reaction models in Eulerian multiphase model. However, their work makes certain considerations that could affect the precision of the results, such as the suppression of a free surface and a slag layer behavior which programed as a function. According to [23] it does not correctly simulate the dissipation of turbulent kinetic energy and therefore, affects the mass transfer between the steel and slag. Currently there have been too few studies [13,17,20,21] that have used the Eulerian multiphase model to simulate multiphase systems of the ladle furnace. Last studies add external codes to solve kinetics of chemical reactions, conducting in the following drawbacks: high computational-costs, greater complexity, time and money. For the contrary, in this work, a simple study of mass transfer during the injection of argon gas was developed. Two Ansys Fluent® pre-loaded models (MTM and MTM+CRM) for the desulfurization were used to well-predict the sulfur removal rates, this new proposed methodology to track desulfurization rate in steel in agitated ladles by gas bottom injection avoids high computational cost compared to using complex thermodynamics-kinetics and flow dynamics coupled models.

2. METHODOLOGY

2.1 MATHEMATICAL MODELS

2.1.1 Computational domain

Figure 1 shows the axisymmetric geometry used to represent the complete axisymmetric domain of the ladle as well as the boundary conditions. The initial conditions of the simulation were stated as follows: there were no concentration gradients of the species, the slag layer had a uniform thickness, slag open eye diameter remained constant once reached its maximum aperture, the temperature and element distribution are homogeneous throughout the ladle. The initial concentration of sulfur in the steel was varied with values of 0.022 and 0.031 wt. %, basados en un estudio previo con metodología y condiciones similares a las desarrolladas en este trabajo [15].

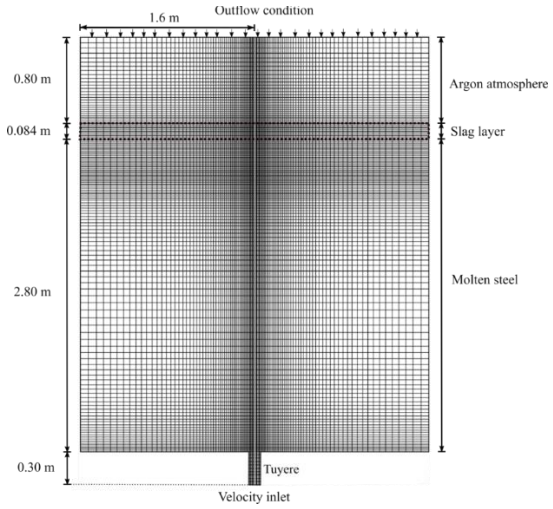

Figure 1. Computational mesh, dimensions and boundary conditions

ISSN: 0012-7361 eISSN: 1989-1490 / DYNA March – April 2022 Vol.97 No 2 DOI: https://doi.org/10.6036/10206

2.1.2 Governing equations

The Eulerian multiphase model was used [24], thus the following equations were solved.

The conservation of the mass for the phase q will be described by Eq. (1):

$$\frac{\partial}{\partial t}\left(\alpha_q \rho_q\right)+\nabla\cdot\left(\alpha_q \rho_q \vec{v}_q\right)=\sum_{p=1}^{n}\left(\dot{m}_{pq}-\dot{m}_{qp}\right) \tag{1}$$

where ρ_q is the density of the phase *q* (kg·m^{-3}); $\vec{v}_q$ is the velocity of the phase *q* (m·s^{-1}); $\dot{m}_{pq}$ is the mass transfer from the phase p^{th} to the phase q^{th} (kg); $\dot{m}_{qp}$ is the mass transfer from the phase q^{th} to the phase p^{th} (kg); α_q is the volumetric fraction of the phase *q*; and *n*, is the total number of phases in the system [24].

Eq. (2) describes the efforts and the momentum within the domain for phase *q*:

$$\frac{\partial}{\partial t}\left(\alpha_q \rho_q \vec{v}_q\right)+\nabla\cdot\left(\alpha_q \rho_q \vec{v}_q \vec{v}_q\right)=-\alpha_q \nabla p+\nabla\cdot\bar{\bar{\tau}}_q+\alpha_q \rho_q \vec{g}+\sum_{p=1}^{n}\left(\vec{R}_{pq}\left(\vec{v}_p-\vec{v}_q\right)+\dot{m}_{pq}\vec{v}_{pq}-\dot{m}_{qp}\vec{v}_{qp}\right) \tag{2}$$

where $\bar{\bar{\tau}}$ is the qth stress-strain tensor defined by Eq. (3):

$$\bar{\bar{\tau}}_q=\alpha_q \mu_q\left(\nabla\vec{v}_q+\nabla\vec{v}_q^{\,T}\right)+\alpha_q\left(\lambda_q-\frac{2}{3}\mu_q\right)\nabla\cdot\vec{v}_q\bar{\bar{I}} \tag{3}$$

where μ_q and λ_q are the bulk viscosity and the shear stress of the phase q^{th}; *p* is the pressure shared by all phases (Pa); $\vec{v}_{pq}$, is the interface velocity (m·s^{-1}); $\vec{R}_{pq}$, is the interaction force between phases (N); and $\vec{g}$, is gravitational acceleration (m·s^{-2}) [24].

Based on the transport equations for turbulent kinetic energy (*k*) and its dissipation velocity (*ε*), the turbulence model *k*-*ε* standard solves Eq. (4) and Eq. (5) for phase *q* [25]:

$$\frac{\partial}{\partial t}(\alpha_q \rho_q k_q)+\nabla\cdot\left(\alpha_q \rho_q \vec{U}_q k_q\right)=\nabla\cdot\left(\alpha_q\left(\frac{\mu_{t,q}}{\sigma_k}\right)\nabla k_q\right)+\alpha_q G_{k,q}-\alpha_q \rho_q \varepsilon_q+\alpha_q \rho_q \Pi_{k_q} \tag{4}$$

$$\frac{\partial}{\partial t}(\alpha_q \rho_q \varepsilon_q)+\nabla\cdot\left(\alpha_q \rho_q \vec{U}_q \varepsilon_q\right)=\nabla\cdot\left(\alpha_q\left(\mu_q+\frac{\mu_{t,q}}{\sigma_\varepsilon}\right)\nabla\varepsilon_q\right)+\alpha_q\frac{\varepsilon_q}{k_q}\left(C_{1\varepsilon}G_{k,q}-C_{2\varepsilon}\rho_q\varepsilon_q\right)+\alpha_q \rho_q \Pi_{\varepsilon_q} \tag{5}$$

The terms Π_{k_q} and Π_{ε_q}, represent the influence of the dispersed phase in the continuous phase *q*; and $G_{k,q}$, is the production of turbulent kinetic energy. The turbulent viscosity ($\mu_{t,q}$) is written as a function of the turbulent kinetic energy (*k*) of the phase *q*, as shown in Eq. (6):

$$\mu_{t,q}=\rho_q C_\mu \frac{k_q^2}{\varepsilon_q} \tag{6}$$

the constants values are $C_{1\varepsilon}$ = 1.44, $C_{2\varepsilon}$ = 1.92, σ_k = 1.0, σ_ε = 1.3 and C_μ = 0.09 [25].

The terms Π_{k_q} and Π_{ε_q} are calculated using the Troshko-Hassan model [26] to represent the effect on the turbulence of the dispersed phase in the continuous phase, which uses Eq. (7) and Eq. (8):

ISSN: 0012-7361 eISSN: 1989-1490 / DYNA March – April 2022 Vol.97 No 2 DOI: https://doi.org/10.6036/10206

$$\Pi_{k_q} = C_{ke} \sum_{p=1}^{M} \frac{K_{pq}}{\alpha_q \rho_q} \left| \vec{U}_p - \vec{U}_q \right|^2 \tag{7}$$

$$\Pi_{\varepsilon_q} = C_{td} \frac{1}{\tau_p} \Pi_{k_q} \tag{8}$$

C_{ke} and C_{td} are two constants whose values are 0.75 and 0.45, respectively. $\vec{U}_p$ and $\vec{U}_q$ are the phase-weighted velocity for phase *p* and *q*, respectively. τ_p, it is the characteristic time of induced turbulence. K_{pq} is the interphase momentum exchange coefficient [24].

Drag force is the force of opposition to the movement in a bubble rising inside a fluid and has an impact on the speed of the uprising bubble as well as on their shape. Therefore, it is necessary to include this force within the simulation [27]. The coefficient of exchange of interfacial momentum between the phases *q* and *p* is described by Eq. (9):

$$K_{pq} = \frac{\rho_p f}{6\tau'_p} d_p A_i \tag{9}$$

where A_i, is the interfacial area; d_p, is the diameter of the bubble of phase *p*; τ'_p, it is the particular relaxation time; and *f*, is a drag function described by Eq. (10):

$$f = \frac{C_D \, \mathrm{Re}}{24} \tag{10}$$

The term Re is the Reynolds number and C_D is the drag coefficient, which is calculated according to the conditions defined in the following criteria Eq. (11) [24]:

$$C_D = \begin{cases} \frac{24}{\mathrm{Re}}\left(1 + 0.15\,\mathrm{Re}^{0.687}\right) \Rightarrow \mathrm{Re} \le 1000 \\ 0.44 \Rightarrow \mathrm{Re} > 1000 \end{cases} \tag{11}$$

Lift effect was included using Tomiyama lift model [28]. According to this model, lift force is determined by Eq. (12):

$$\vec{F}_{lift} = -C_l \rho_q \alpha_p \left(\vec{v}_q - \vec{v}_p\right) \times \left(\nabla \times \vec{v}_q\right) \tag{12}$$

where C_l is lift coefficient and it is calculated according to Eq. (13)-(17):

$$C_l = \begin{cases} \min\left[0.288 \tanh\left(0.121 \mathrm{Re}_p\right), f\left(Eo'\right)\right] & Eo' \le 4 \\ f\left(Eo'\right) & 4 < Eo' \le 10 \\ -0.27 & 10 < Eo' \end{cases} \tag{13}$$

$$f\left(Eo'\right) = 0.00105 Eo'^3 - 0.0159 Eo'^2 - 0.0204 Eo' + 0.474 \tag{14}$$

$$Eo' = \frac{g\left(\rho_q - \rho_p\right) d_h^2}{\sigma} \tag{15}$$

$$d_h = d_b \left(1 + 0.163 Eo^{0.757}\right)^{1/3} \tag{16}$$

ISSN: 0012-7361 eISSN: 1989-1490 / DYNA March – April 2022 Vol.97 No 2 DOI: https://doi.org/10.6036/10206

$$Eo = \frac{g\left(\rho_q - \rho_p\right)d_b^2}{\sigma} \tag{17}$$

Eo represents Eötvös number, dimensionless; this number relates buoyancy and surface tension forces. Eo' is a modified Eötvös number and it is based on the longer axis of the bubble, d_h. σ is surface tension, N·m^{-1}; g is gravity acceleration, m·s^{-2}; and d_b is bubble diameter.

The force due to turbulent dispersion effect is modeled using Burns et al. model [29]. Here, the scalar dispersion, D_{tq}, is calculated with Eq. (18):

$$D_q = D_p = D_{tq} = \frac{\mu_{tq}}{\rho_q} \tag{18}$$

where D_q and D_p are scalar dispersion of continuous and disperse phase, respectively. Thus, turbulent dispersion force can be determined by Eq. (19):

$$\vec{F}_{td,q} = -\vec{F}_{td,p} = C_{TD}K_{pq}\frac{D_q}{\sigma_{pq}}\left(\frac{\nabla\alpha_p}{\alpha_p} - \frac{\nabla\alpha_q}{\alpha_q}\right) \tag{19}$$

σ_{pq} is dispersion Prandtl number and its value is 0.9; C_{TD} constant value is set to 1[29].

For turbulent flows, the mass diffusion of specie *i* is computed by Eq. (20) [24]:

$$\vec{J}_i = -\left(\rho D_{i,m} + \frac{\mu_t}{Sc_t}\right)\nabla Y_i - D_{T,i}\frac{\nabla T}{T} \tag{20}$$

where $D_{m,i}$ is mass diffusion coefficient for specie *i* in the mixture, Y_i is local mass fraction of specie *I* and $D_{T,i}$ is the thermal diffusion coefficient (in this case, equal to 0). Sc_t is the turbulent Schmidt number which is defined by Eq. (21):

$$Sc_t = \frac{\mu_{t,q}}{\rho D_t} \tag{21}$$

D_t is turbulent diffusion for specie *i*.

The unidirectional mass transfer between two phases is defined as a positive variation of the mass flow per unit volume from phase *p* to phase *q*, which is determined by Eq. (22) [24]:

$$\psi_{pq} = \dot{r}\alpha_p y_{p,i}\rho_q \tag{22}$$

where $\dot{r}$ is a constant rate of particle shrinking; and $y_{p,i}$ is the mass fraction of species *i* in the *p* phase. To calculate $\dot{r}$, the stirring power generated by the injected gas plume was used, according Eq. (23) [30]:

$$\dot{\varepsilon} = 14.23\left(\frac{Q_g \cdot T}{M}\right)\cdot\log\left(1 + \frac{H}{1.48\cdot P_0}\right) \tag{23}$$

where $\dot{\varepsilon}$ is the stirring power of the gas (W·t^{-1}) in ladle; Q_g, is the incoming gas flow (Nm^3·min^{-1}); M, is the steel mass in tons; T, is the temperature in Kelvin; H, is the depth of the gas injection (m); and P_0 (atm), is the pressure on the surface of the bath.

Using stirring power, it is possible to calculate the velocity constant k_s (s^{-1}) by means of Eq. (24) [31]:

ISSN: 0012-7361 eISSN: 1989-1490 / DYNA March – April 2022 Vol.97 No 2 DOI: https://doi.org/10.6036/10206

$$\text{if } \begin{cases} \dot{\varepsilon} < 60 \text{ W} \cdot \text{ton}^{-1} \Rightarrow k_s \approx 0.013\dot{\varepsilon}^{0.25} \\ \dot{\varepsilon} > 60 \text{ W} \cdot \text{ton}^{-1} \Rightarrow k_s \approx 8\times10^{-06}\dot{\varepsilon}^{2.1} \end{cases} \tag{24}$$

Eq. (25) relates the velocity constant with the mass transfer coefficient K, (m·s^{-1}) as follows [32]:

$$K = k_s\left(\frac{V_{steel}}{A_i}\right) \tag{25}$$

where V_{steel} (m^3) is the volume of the steel in the ladle; and A_i is the interfacial area between the steel and the slag (m^2). For the calculation of the mass transfer rate of sulfur between steel and slag, Eq. (26) was used [33]:

$$\dot{n} = KA_i\left(C_f - C_i\right) \tag{26}$$

where $\dot{n}$ is the mass transfer rate (kg·s^{-1}); and both C_i and C_f are the initial and final concentrations of sulfur in the steel (kg·m^{-3}), respectively. As a requirement of the computational program, the emission rate of the source term, $\dot{r}$ (kg·m^{-3}·s^{-1}) was calculated by the following Eq. (27):

$$\dot{r} = \frac{\dot{n}}{V_{(steel)}} \tag{27}$$

The chemical reaction of desulfurization -carried out with calcium oxide- was simulated according to the reaction described by Eq. (28) [32]:

$$\text{CaO} + \text{S} \rightarrow \text{CaS} + \text{O} \tag{28}$$

By using the Arrhenius model, described in Eq. (29), it is possible to determine the rate constant of reaction, k_c, as follows:

$$k_c = Ae^{\left(\frac{-E_a}{\text{R}\cdot T}\right)} \tag{29}$$

where A is the frequency factor (s^{-1}), E_a is the activation energy (kJ·mol^{-1}), R is the universal gas constant (kJ·mol^{-1}·K^{-1}) and T is temperature (K). In laminar flow regions, as well as low velocity steel zones, Arrhenius equation is employed to calculate the constant of chemical reaction. For turbulent zones, this approximation is also used, but in this case, the eddy dissipation model has also to be solved. The production, R_i, of specie i for reaction r considers the mixing time scale (which relate ε and k). The model is shown in Eq. (30) and (31) [34].

$$R_{i,r} = \nu'_{i,r}M_w A\rho\frac{\varepsilon}{k}\min_{\Re}\left(\frac{Y_{\Re}}{\nu'_{\Re,r}M_{w,\Re}}\right) \tag{30}$$

$$R_{i,r} = \nu'_{i,r}M_{w,i}AB\rho\frac{\varepsilon}{k}\frac{\sum_P Y_P}{\sum_j^N \nu''_{j,r}M_{w,j}} \tag{31}$$

Here, Y_p and $Y_{\Re}$ are mass fractions of specie product P and reactant $\Re$, respectively. A and B are constants whose values are 4.0 and 0.5, respectively [34]. In this model, the production rate is calculated by the smaller value of the two equations.

2.1.3 Assumptions, boundary conditions and material properties

The computational mesh employed 8056 elements, which was refined in the steel-slag interface, as well as in the plume zone. Grid size was determined using mesh sensibility technique. Different meshes were tried (from 2000 to 50000 elements) and its effects on

ISSN: 0012-7361 eISSN: 1989-1490 / DYNA March – April 2022 Vol.97 No 2 DOI: https://doi.org/10.6036/10206

velocity results were measured. Also, different structure-types were considered and 100% orthogonality gave better results. The water axial velocity was used as response variable with different grid refinement and beyond 8056 elements there was not a significant difference. The following considerations were made for the simulation: the calculations were made in transient and isothermal state, the gas flow was constant and injected at the center of the bottom ladle through a tuyere, gas bubbles were spherical and constant diameter, and there was no-reaction between steel and gas. Initial concentrations of oxygen in steel were set to 0.00044 wt. % according to L. Jonsson et.al [15]. For slag, the chemical composition was CaO 55 wt. %, Al_2O_3 30 wt. %, MgO 7.5 wt. % and SiO_2 7.5% wt. as well as L. Jonsson et.al [15]. Table 1 shows the properties of the steel, slag and argon used in the simulations and shows the forces included in each case.

Properties	Value
Steel density [14]	7020 $kg \cdot m^{-3}$
Slag density [14]	3500 $kg \cdot m^{-3}$
Argon density [14]	1.6228 $kg \cdot m^{-3}$
Steel-slag surface tensión [14]	1.15 $N \cdot m^{-1}$
Steel-argon surface tension [14]	1.82 $N \cdot m^{-1}$
Slag-argon surface tensión [14]	0.58 $N \cdot m^{-1}$
Viscosity of steel [14]	0.0055 Pa·s
Viscosity of slag [14]	0.06 Pa·s
Viscosity of argon [14]	2.125×10^{-05} Pa·s
Argon bubble diameter	0.01 m
Diffusivity of sulfur in slag [14]	1×10^{-10} ($m^2 \cdot s^{-1}$)
Diffusivity of sulfur in steel [14]	4.43×10^{-08} ($m^2 \cdot s^{-1}$)
Cases configuration for fluid dynamics	
Case	**Force**
1	Drag force, Buoyancy force, Surface tension
2	Drag force, Lift force, Turbulent dispersion force, Buoyance force, Surface tension force

Table 1. Properties of materials used in simulation and cases configuration.

Two different cases were proposed to compare drag and non-drag forces effects. Case 1 is a simple configuration and Case 2 includes all forces related to gas ladle stirring process. The equations were solved with ANSYS Fluent 15.0® CFD software. The solution method employed was the Phase coupled SIMPLE, using convergence criteria of 1×10-04 for each variable. A workstation equipped with an Intel® Xeon® E3-1241 v3 processor was used for simulation.

3. RESULTS

The proposed fluid-dynamics model was validated through the results expressed on literature [36] on which a scale model (1:17) of the ladle was employed, using a three-phase system (water/oil/air) in order to represent the behavior of steel, slag and argon. To validate the fluid dynamics obtained by numerical modeling it was employed the technique of Particle Image Velocimetry (PIV), this technique was described in previous work [37]. In Figure 2 the experimental axial velocities were compared with the numerical axial velocities through the radial distance for different heights: z = 4, 8, 12 and 16 cm. At low heights (4 and 8 cm) the agreement is better and on the other hand, this is lower near the free surface. PIV technique takes in account all phenomena occurred in a multiphase system, nevertheless, CFD omitted in this case, bubble deformation, agglomeration, break-up and coalescence; this affects the adjustment up to certain extent, and therefore it was chosen a tendency-based agreement.

ISSN: 0012-7361 eISSN: 1989-1490 / DYNA March – April 2022 Vol.97 No 2 DOI: https://doi.org/10.6036/10206

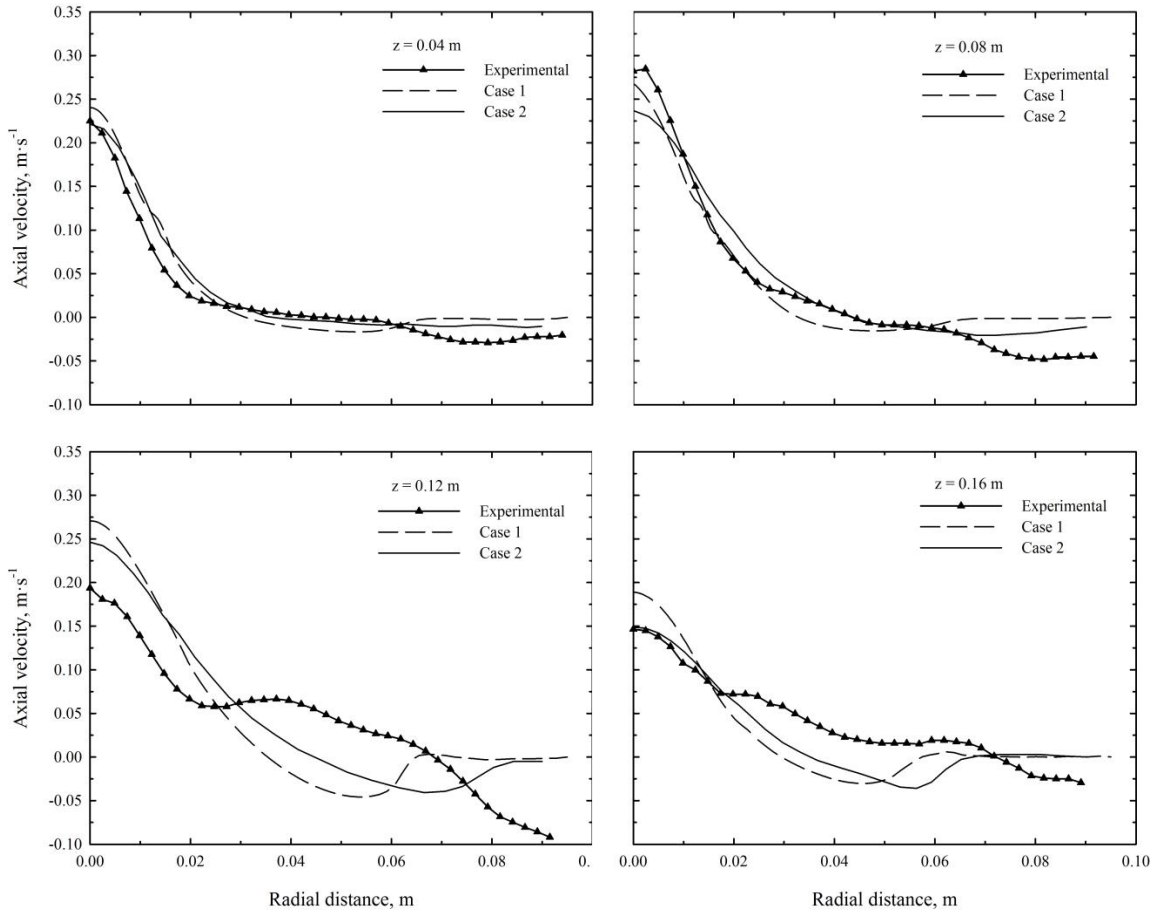

Figure 2. Radial distribution of axial velocity at different heights for both cases.

In Figure 3 the steel velocity vectors of the two cases are shown at different times for the same gas flow rate. The highest velocities of the steel are located mainly in the region of the plume in both cases, however case 2 has a slightly lower ascending rate. Initially, in both cases the plume begins to develop from the first seconds of injection and there is the formation of two recirculations near the tip of the gas column (points A and A'). At 3 s, the plume has increased its height and moved the recirculations as indicated by points B and B'. In case 1, at this time the plume has reached the free surface of the steel, while in case 2, it is located above the middle of steel height. This difference in velocities is due to the incorporation of the turbulent dispersion force in case 2, which produces the spreading of the ascending gas velocity and therefore reduces the turbulent kinetic energy. At 9 s of injection, the plume has fully developed in both cases, however, the fluid dynamic behavior at the free surface is different between them. In case 1, the eruption of the plume is homogeneous and does not produce many disturbances in the steel. On the other hand, in case 2, the gas plume produces a greater movement of the steel on the free surface and causes the formation of regions of high velocity close to the walls. The shapes of the recirculations established in case 1 are well defined (points C), while in case 2 they are deformed as a result of the reintroduction of the steel (points C'). Finally, the quasi-stable state is reached after 15 s simulation and case 1 reported a more defined and smoothed flow dynamics structure with the formation of two recirculations adjacent to the gas plume (points D). On the other hand, in case 2 the fluid dynamics structure of the steel is completely different with a more marked reintroduction of the steel phenomenon. Finally, the recirculations formed in this case are further from the plume (points D').

ISSN: 0012-7361 eISSN: 1989-1490 / DYNA March – April 2022 Vol.97 No 2 DOI: https://doi.org/10.6036/10206

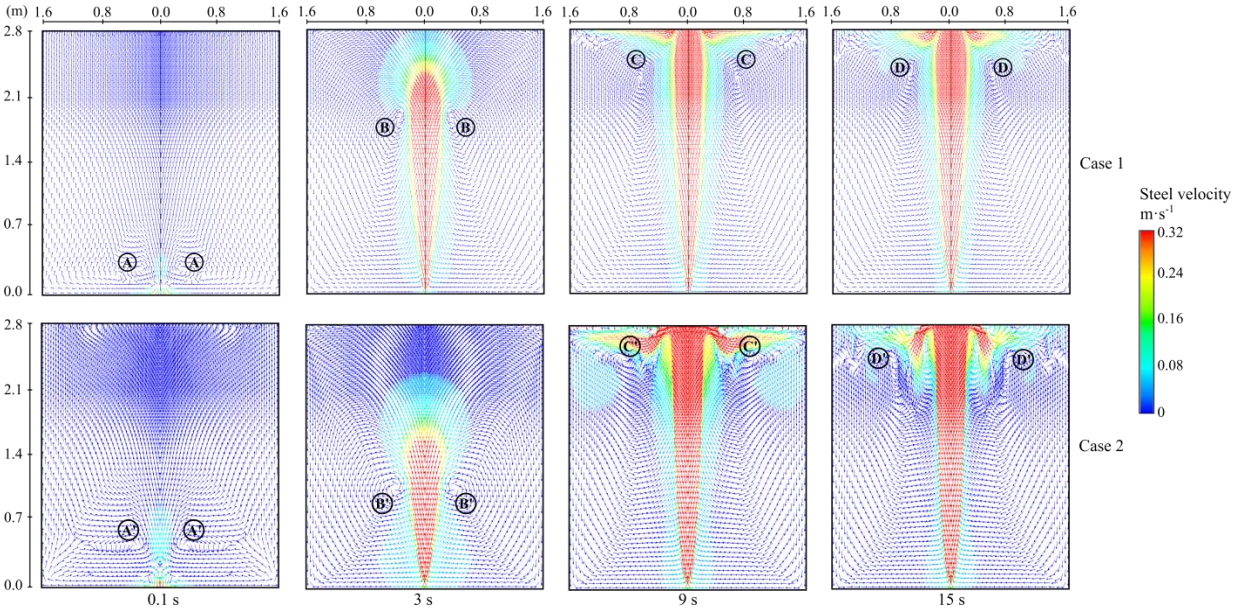

Figure 3. Fluid dynamics structure of steel at different time in the axisymmetric plane for both cases using 500 Nl·min^{-1} gas flow.

When using MTM to calculate sulfur mass transfer, it was necessary to calculate, employing Eqs. (15)-(19), the emission rate of the source term for both gas flows were 1.07×10^{-03} kg·m^{-3}·s^{-1} and 1.23×10^{-03} kg·m^{-3}·s^{-1}, respectively. To calculate the rate of sulfur mass transfer by using CRM, the Eq. (29) was employed. This equation was transformed by the properties of the logarithms to obtain the ln k against inverse of the temperature from literature [38], and the calculated values were: E_a= 104.6 kJ·mol^{-1} and A= 0.4130 s^{-1}.

To validate desulfurization rate, Figure 4 compares the complete model predictions from Case 2 with experimental literature data [39], observing good adjustment in final values by both techniques. Though, it is also observed with curves slope that desulfuration rate is faster in experimental data at first 260 s. This result probably can be better predicted by using more robust models for chemical kinetics that include thermodynamics interaction parameters and temperature variations, however, it was out of this research aims. Figure 5 shows the variation of the sulfur content against refining time for four cases: in two, it was used the Mass Transfer Model (MTM); and in the other two, MTM was used in combination with the Chemical Reaction Model (CRM). It can be seen a similar behavior in the decrease of the sulfur content for all cases with different initial sulfur concentration. However, the lowest sulfur content is obtained when only the MTM was used, reaching a content of sulfur of 0.01 wt. % with 500 Nl·min^{-1} of argon gas injection. When the CRM is used in conjunction with the MTM, it was found that the gas flow causes a slight difference between the final sulfur content. This difference between the different mechanisms occurs because there is a gradual decrease in the sulfur content which leads to a decrease in the rate of chemical reaction. Therefore, the consumption of sulfur is lower, as observed in the cases that employ the Chemical Reaction Model. It can also be seen that, regardless of the approach used, the rate of desulfurization is always higher as greater argon flows are used, as expected owing to the stirring state of steel.

ISSN: 0012-7361 eISSN: 1989-1490 / DYNA March – April 2022 Vol.97 No 2 DOI: https://doi.org/10.6036/10206

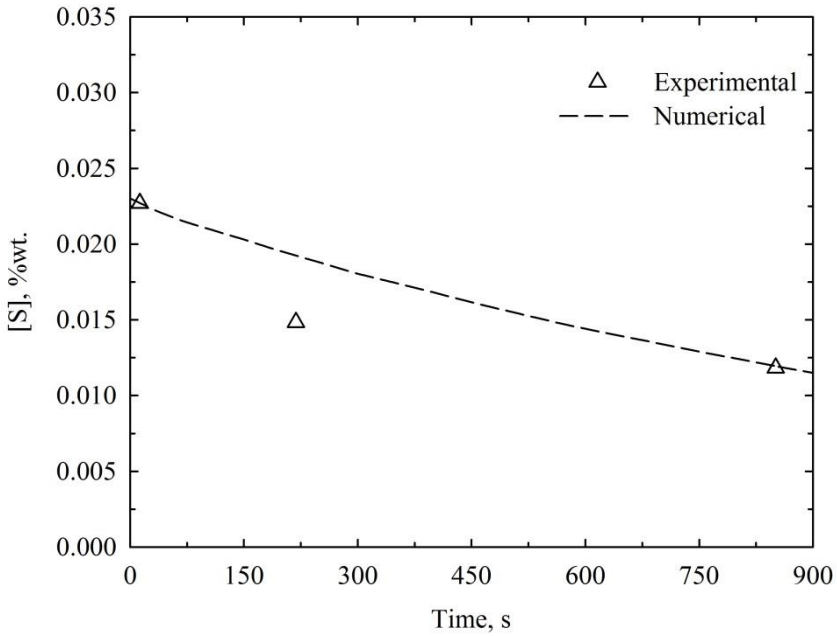

Figure 4. Sulfur content calculated by experimental [39] and numerical technique (Case 2).

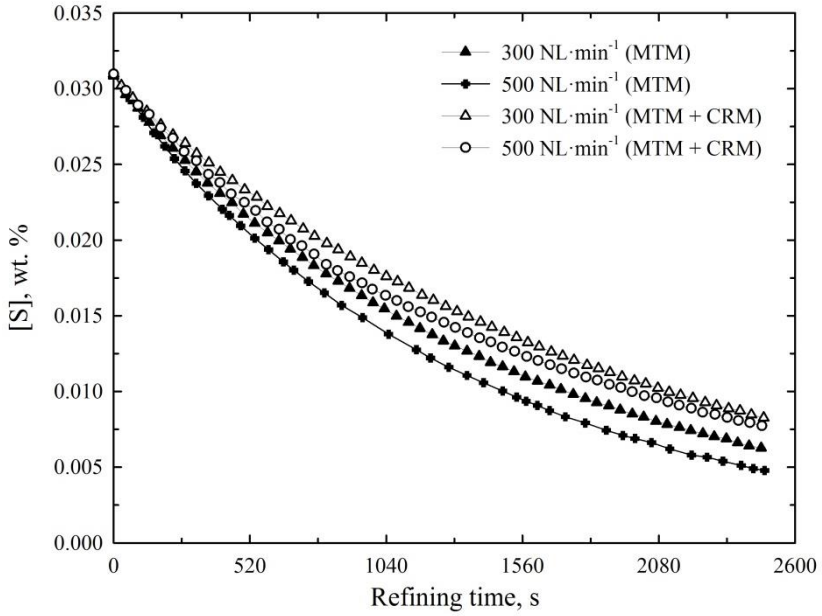

Figure 5. Sulfur variation in steel with the studied gas flows and the numerical models.

ISSN: 0012-7361 eISSN: 1989-1490 / DYNA March – April 2022 Vol.97 No 2 DOI: https://doi.org/10.6036/10206

Figure 6 compares the effect of the initial sulfur content for the two studied cases. It is clearly observed that incorporation of drag forces did not significantly affects the desulfurization rate, however, the decrease in the initial sulfur content reduced the sulfur removal rate. Hence, reducing the sulfur concentration gradient slows the removal rate due to the generation of a lower driving force.

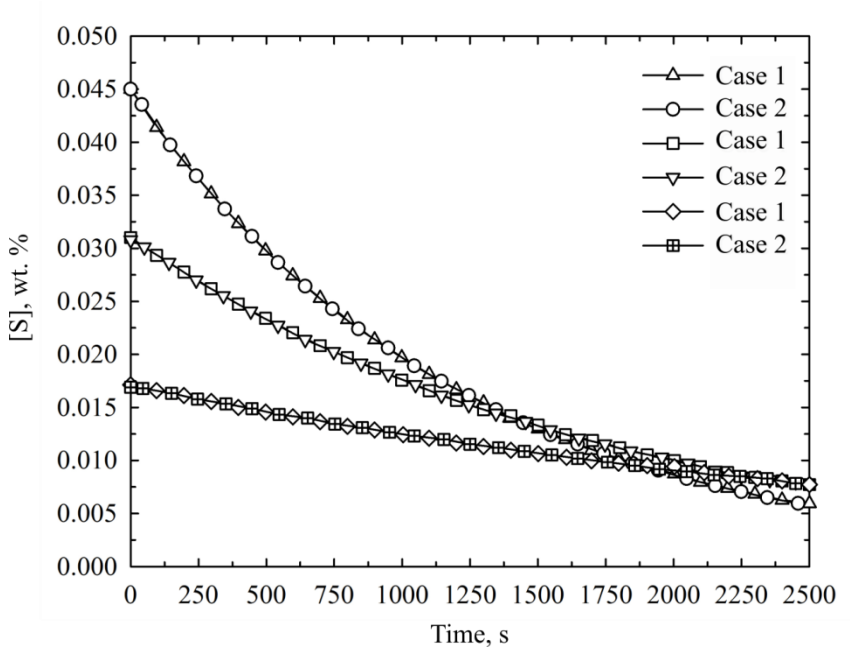

Figure 6. Effect of forces and initial sulfur content on desulfuration rate

Figure 7 shows the sulfur contained in the steel and in the slag at different times by using the MTM and MTM + CRM models for Case 2. In both approaches, a decrease in sulfur into the entire volume of the steel is noticeable. However, by using only the mass transfer model (Figure 7a), a lower amount of sulfur is achieved than when the mass transfer and chemical reaction models are combined (Figure 7b). This behavior is attributed to the fact that the reaction rate is defined by the remnant concentration of sulfur and therefore decreases as it reacts. The content of sulfur transferred to the slag by means of the mass transfer mechanism (Figure 7c) shows that the exchange occurs mainly in the areas close to the walls of the ladle due to disturbances of the steel. In addition, there is a slight increase in sulfur of steel due to the small reintroduction of slag. On the other hand, the sulfur present in the slag using the combined MTM + CRM is determined through the formation of CaS (Figure 7d). Here it is clear that the main area where sulfide occurs is at the opening of the slag layer, where agitation enhances steel-slag interaction, and it advances along time throughout the areas of steel-slag contact.

ISSN: 0012-7361 eISSN: 1989-1490 / DYNA March – April 2022 Vol.97 No 2 DOI: https://doi.org/10.6036/10206

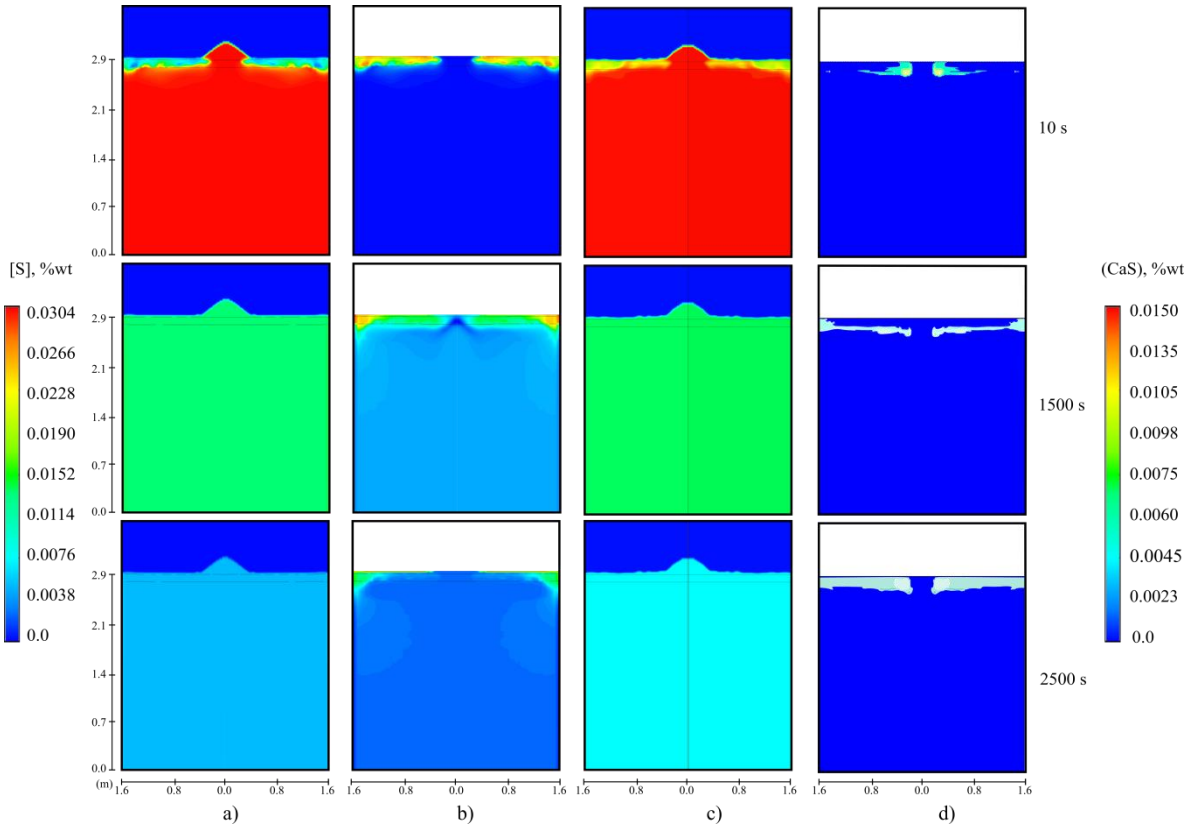

Figure 7. Sulfur concentration at different times in steel through a) MTM and c) MTM+CRM, and sulfur content in slag calculated by b) MTM and d) MTM+CRM.

4. CONCLUSIONS

In the present work the flow dynamics and sulfur mass transfer from steel to slag with drag and non-drag forces were numerically simulated. A concentric gas stirring of the steel in the ladle by using different flow rates of argon gas was achieved, and then available mass transfer and chemical reaction models in Ansys Fluent ® v.15 were tested, the conclusions of this study are given as follows:

1. Fluid-dynamics results have shown an acceptable agreement with those obtained experimentally by using the well-known PIV technique in a scale model.

2. Despites simplicity and low-computational cost approaches of mass transfer and chemical reaction models, good agreement in the final sulfur values with published experimental ones were observed.

3. Desulfurization rates by using an argon flow of 500 Nl·min^{-1} are greater than those obtained with a flow of 300 Nl·min^{-1}, for the two approaches used, MTM and MTM in combination with CRM.

4. The highest rate of desulfurization occurs in the first seconds of the process in the region of the opening of the slag layer, where the convective mechanism is the main driver of the desulfurization reaction. However, in the region near the wall of the ladle a stagnation zone of steel prevails the diffusive mechanism.

5. By employing MTM, it was obtained ~15% less sulfur than that obtained with the MTM+CRM at the end of the simulation. The above is attributed to the decrease of the reactants as the reaction evolves, which does not occur in the MTM. This result is more realistic and, furthermore will allow to simulate the steel refining process in a better way for future works.

ISSN: 0012-7361 eISSN: 1989-1490 / DYNA March – April 2022 Vol.97 No 2 DOI: https://doi.org/10.6036/10206

NOMENCLATURE

Symbol	Description
A	Frequency factor, s^{-1}
A_i	Interfacial area, m^2
$C_{1\varepsilon}$, $C_{2\varepsilon}$, C_μ	Constants of turbulence model, dimensionless
C_{ke}, C_{td}	Constants of turbulent interaction model, dimensionless
C_D	Drag coefficient, dimensionless
C_i, C_f	Initial and final concentrations, %wt.
D_i	Mass diffusion coefficient of specie i, $m^2 \cdot s^{-1}$
D_t	Turbulent mass diffusion coefficient of specie i, $m^2 \cdot s^{-1}$
d_p	Diameter of bubble, m
E_a	Energy activation, $kJ \cdot mol^{-1}$
f	Drag function, dimensionless
G_k	Production of turbulent kinetic energy, $m^2 \cdot s^{-2}$
g	Gravity acceleration, $m \cdot s^{-2}$
H	Ladle height, m
J_i	Mass flux of specie i, $kg \cdot m^{-2} \cdot s^{-1}$
K	Mass transfer coefficient, min^{-1}
K_{pq}	Interphase momentum exchange coefficient between p and q, dimensionless
k	Turbulent kinetic energy, $J \cdot kg^{-1}$
k_c	Constant of chemical reaction, s^{-1}
k_s	Mass transfer constant, $m \cdot s^{-1}$
M	Mass of steel, ton
$\dot{m}$	Mass flow rate between phases, $kg \cdot s^{-1}$
$\dot{n}$	Mass transfer rate, $kg \cdot s^{-1}$
P_0	Atmospheric pressure, atm
p	Pressure, Pa
q^{th}	Phase q, dimensionless
Q	Flow rate of gas injection, $m^3 \cdot min^{-1}$
R	Universal gas constant, $kJ \cdot mol^{-1} \cdot K^{-1}$
$\vec{R}$	Interaction force between phases, N
$\dot{r}$	Mass emission rate, $kg \cdot m^{-3} \cdot s^{-1}$
Re	Reynolds number, dimensionless
Sc_t	Turbulent Schmidt number, dimensionless
T	Temperature, K
U	Phase-weighted velocity, $m \cdot s^{-1}$
V	Volume of steel in ladle, m^3
v	Velocity, $m \cdot s^{-1}$
Y_i	Local mass fraction of specie i, dimensionless
Greek Symbols	
α	Volume fraction, dimensionless
ε	Turbulent dissipation rate, $m^2 \cdot s^{-3}$
$\dot{\varepsilon}$	Stirring power, $W \cdot ton^{-1}$
λ	Bulk viscosity, Pa·s
μ	Dynamic viscosity, Pa·s
Π	Influence of disperse phase in continuous phase, dimensionless
ρ	Density, $kg \cdot m^{-3}$
τ	Characteristic time, s
$\overline{\overline{\tau}}$	Stress-strain tensor, Pa
ψ_{pq}	Unidirectional mass transfer, $kg \cdot s^{-1}$

ISSN: 0012-7361 eISSN: 1989-1490 / DYNA March – April 2022 Vol.97 No 2 DOI: https://doi.org/10.6036/10206

REFERENCES

[1] A. Senguttuvan and G. Irons, "Modeling of slag entrainment and interfacial mass transfer in gas stirred ladles," *ISIJ International*, vol. 57, no. 11, pp. 1962-1970, 2017. DOI: https://doi.org/10.2355/isijinternational.ISIJINT-2016-589

[2] M. Nakai, Y. Murata, M. Morinaga, and R. Hashizume, "Effect of impurity sulfur on the formation of Cr_2O_3 and SiO_2 at the early stage of steam oxidation in both ferittic and austenitic steels", *Material Transactions*, vol. 44, no. 9, pp. 1830-1838, 2003. DOI: https://doi.org/10.2320/matertrans.44.1830

[3] A. Matsui, Y. Uchida, N. Kikuchi, and Y. Miki, "Effects of temperature and oxygen potential on removal of sulfur from desulfurization slag", *ISIJ International*, vol. 57, no. 6, pp. 1012-1018, 2017. DOI: https://doi.org/10.2355/isijinternational.ISIJINT-2016-748

[4] D. Mazumdar and R. Guthrie, "The physical and mathematical modelling of gas stirred ladle systems," *ISIJ International*, vol. 35, no. 1, pp. 1-20, 1995. DOI: https://doi.org/10.2355/isijinternational.35.1

[5] P. Jönsson and T. Jonsson, "The use of fundamental process models in studying ladle refining operations," *ISIJ International*, vol. 41, no. 11, pp. 1289-1302, 2001. DOI: https://doi.org/10.2355/isijinternational.41.1289

[6] G. Irons, A. Senguttuvan, and K. Krishnapisharody, "Recent advances in the fluid dynamics of ladle metallurgy," *ISIJ International*, vol. 55, no. 1, pp. 1-6, 2015. DOI: https://doi.org/10.2355/isijinternational.55.1

[7] M. Radune, A. Radune, F. Assous, M. Zinigrad, and D. Eliezer, "Investigation of sulfur transition through metal-slag phase boundary in natural moving conditions," *Defect and Diffusion Forum*, vol. 273-276, pp. 752-756, 2008. DOI: https://doi.org/10.4028/www.scientific.net/DDF.273-276.752

[8] L. Teixeira and R. Parreiras, "Multiphase mass transfer in iron and steel refining processes," *Mass transfer- Advancement in process modelling*, M. Solecki, Ed. Minas Gerais, Brasil: INTECH, ch. 7, pp. 149-167, 2015. DOI: https://doi.org/10.5772/60800

[9] A. Conejo, F. Lara, M. Macias-Hernandez, and R. Morales, "Kinetic model of steel refining in a ladle furnace," *Steel Research International*, vol. 78, no. 2, pp. 141-150, February 2007. DOI: https://doi.org/10.1002/srin.200705871

[10] L. Jonsson and P. Jönsson, "Modeling of fluid flow conditions around the slag/metal interface in a gas-stirred ladle," *ISIJ International*, vol. 36, no. 9, pp. 1127-1134, 1996. DOI: https://doi.org/10.2355/isijinternational.36.1127

[11] C. Llanos, S. García, A. Ramos, J. Barreto, and G. Solorio, "Multiphase modeling of the fluidynamics of bottom Argon bubbling during ladle operations," *ISIJ International*, vol. 50, no. 3, pp. 396-402, 2010. DOI: https://doi.org/10.2355/isijinternational.50.396

[12] M. Peranandhanthan and D. Mazumdar, "Modeling of slag eye area in argon steel ladles," *ISIJ International*, vol. 50, no. 11, pp. 1622-1631, 2010. DOI: https://doi.org/10.2355/isijinternational.50.1622

[13] W. Lou and M. Zhu, ""Numerical simulations of inclusion behavior and mixing phenomena in gas-stirred ladles with different arrangement of tuyeres"," *ISIJ International*, vol. 54, no. 1, pp. 9-18, 2014. DOI: https://doi.org/10.2355/isijinternational.54.9

[14] H. Liu, Z. Qi, and M. Xu, "Numerical simulation of fluid flow and interfacial behavior in three-phase Argon-stirred ladles with one plug and dual plugs," *Steel Research*, vol. 82, no. 4, pp. 440-458, 2011. DOI: https://doi.org/10.1002/srin.201000164

[15] L. Jonsson, D. Sichen, and P. Jönsson, "A new approach to model sulphur refining in a gas-stirred ladle – a coupled CFD and thermodynamic model.," *ISIJ International*, vol. 38, no. 3, pp. 260-267, 1998. DOI: https://doi.org/10.2355/isijinternational.38.260

[16] M. Andersson, L. Jonsson, and P. Jönsson, "A thermodynamic and kinetic model of reoxidation and desulphurisation in the ladle furnace," *ISIJ International*, vol. 40, no. 11, pp. 1080-1086, 2000. DOI: https://doi.org/10.2355/isijinternational.40.1080

[17] M.N. Al-Harbi, Simulation of ladle degassing in steel making process. Leicester, Reino Unido: ProQuest LLC, 2007. URL: https://leicester.figshare.com/articles/thesis/Simulation_of_ladle_degassing_in_steel_making_process/10138802/1

[18] C. Zhu, P. Chen, G. Li, X. Luo, and W. Zheng, "A mathematical model of desulphurization kinetics for ultra-low sulfur steels refining by powder injection during RH processing," *ISIJ International*, vol. 56, no. 8, pp. 1-10, 2016. DOI: https://doi.org/10.2355/isijinternational.ISIJINT-2016-124

[19] U. Singh, R. Anapagaddi, S. Mangal, K. Padmanabhan, and A. Singh, "Multiphase modeling of bottom-stirred ladle for prediction of slag-steel interface and estimation of desulfurazion behavior," *Metallurgical and Materials Transactions B*, vol. 47, no. 3, pp. 1804-1816, 2016. DOI: https://doi.org/10.1007/s11663-016-0620-2

[20] W. Lou and M. Zhu, "Numerical simulation of gas and liquid two-phase flow in gas-stirred systems based on Euler-Euler approach," Metallurgical and Transactions B, vol. 44, no. 5, pp. 1251-1263, 2013. DOI: https://doi.org/10.1007/s11663-013-9897-6

[21] W. Luo and M. Zhu, "Numerical simulation of desulfurization behavior in gas-stirred systems based on computation Fluid Dynamics–Simultaneous Reaction Model (CFD–SRM) coupled model," *Metallurgical and Materials Transactions B*, vol. 45, no. 5, pp. 1706-1722, 2014. DOI: https://doi.org/10.1007/s11663-014-0105-0

[22] W. Lou and M. Zhu, "Numerical simulation of slag-metal reactions and desulfurization efficiency in gas-stirred ladles with different thermodynamics and kinetics," *ISIJ International*, vol. 55, no. 5, pp. 961-969, 2015. DOI: https://doi.org/10.2355/isijinternational.55.961

[23] Q. Cao and L. Nastac, "Mathematical investigation of fluid flow, mass transfer, and slag-steel interfacial behavior in gas-stirred ladles," *Metallurgical and Materials Transactions B.*, vol. 49, no. 3, pp. 1388-1404, 2018. DOI: https://doi.org/10.1007/s11663-018-1206-y

ISSN: 0012-7361 eISSN: 1989-1490 / DYNA March – April 2022 Vol.97 No 2 DOI: https://doi.org/10.6036/10206

[24] Ansys, Inc. Fluent Theory Guide, ANSYS, Inc., Canonburg, USA, 2013.

[25] B. Launder and D. Spalding, Lectures in mathematical models of turbulence. London, England: Academic Press, 1972.

[26] A.A. Troshko and Y.A. Hassan, "A two-equation turbulence model of turbulent bubbly flows," *International Journal of Multiphase Flow*, vol. 27, no. 11, pp. 1965-2000, 2001. DOI: https://doi.org/10.1016/S0301-9322(01)00043-X

[27] C. Méndez, N. Nigro, and A. Cardona , "Drag and no-drag force influences in numerical simulations of metallurgical ladles," *Journal of Materials Processing Technology*, vol. 160, no. 3, pp. 296-305, 2005. DOI: https://doi.org/10.1016/j.jmatprotec.2004.06.018

[28] A. Tomiyama, "Struggle with computational bubble dynamics," *Multiphase Science and Technology*, vol. 10, no. 4, p. 369, 1998.

DOI: https://doi.org/10.1615/MultScienTechn.v10.i4.40

[29] A.D. Burns, T. Frank, I. Hamill, and J. Shi, "The Favre Averaged Drag Model for Turbulent Dispersion in Eulerian Multi-Phase Flows," *5th. Int. Conf. on Multiphase Flow*, Yokohama, 2004. DOI: https://citeseerx.ist.psu.edu/viewdoc/download?doi=10.1.1.453.2254&rep=rep1&type=pdf

[30] E.T. Tukdogan, Fundamentals of Steelmaking, 1st ed. London: The Institute of Materials, 1996.

[31] S. Asai, I. Muchi, and M. Kawachi, "Fluid flow and mass transfer in gas stirred ladles," *Foundry Processes*. USA, Springer, pp. 261-292, 1988.

DOI: https://doi.org/10.1007/978-1-4613-1013-6_9

[32] R. Fruehan, Ed., "The making, shaping and treating of steel", 11th ed. Pittsburgh, USA: The AISE Steel Foundation, 1998.

[33] L. Holappa, "Secondary Steelmaking," in Treatise on process metallurgy, Industrial Processes, Part A. Coventry, UK: Elsevier, 2014, ch. 1.6, pp. 301-345. DOI:10.1016/B978-0-08-096988-6.00012-2

[34] B.F. Magnussen and B.H. Hjertager, "On mathematical modeling of turbulent combustion with special emphasis on soot formation and combustion," *Symposium (International) on Combustion*, vol. 16, no. 1, pp. 719-729, 1977. DOI: https://doi.org/10.1016/S0082-0784(77)80366-4

[35] L. Muhmood, N. Viswanathan, and S. Seetharaman, "A new approach for the diffusion coefficient evaluation of sulfur in CaO-SiO_2-Al_2O_3 slag," *Deflect and Diffusion Forum*, vol. 312-315, pp. 626-634, 2011. DOI: https://doi.org/10.4028/www.scientific.net/DDF.312-315.626

[36] Luis E. Jardón-Perez, Juan Antonio López-Gutierrez, Alfredo Vázquez, C. González-Rivera, and Marco Aurelio Ramírez-Argaez, "Physical and mathematical of metal-slag exchanges in gas-stirred ladles," *MRS Advances*, vol. 2, no. 61, pp. 3821-3829, 2017. DOI: https://doi.org/10.1557/adv.2017.607

[37] R. González-Bernal et al., "Effect of the fluid-dynamic structure on the mixing time of a ladle furnace," *Steel Research International*, vol. 89, no. 2, p. 1700281, 2018. DOI: https://doi.org/10.1002/srin.201700281

[38] T. Yagi and Y. Ono, "Effects of various factors on the rate of desulfurization of molten pig iron with solid lime.," Tetsu-to-Hagané, vol. 45, no. 11, pp. 1236-1241, 1959. DOI: https://doi.org/10.2355/tetsutohagane1955.45.11_1236

[39] A. Tilliander, M. Ersson, and L.T.I. Jonsson, "Fundamental mathematical modeling of metallurgical processes – current and future situation," in SCANMET III, Lulea, pp. 333-346, 2008. URL: https://www.researchgate.net/publication/233920290_Fundamental_mathematical_modeling_of_metallurgical_processes_-_current_and_future_situation

ACKNOWLEDGMENTS

The authors thank the National Council of Science and Technology (CONACYT) for the scholarship for postgraduate studies of Antonio Urióstegui Hernández, and to TecNM/I.T. Morelia, Cátedras-CONACyT, CIDESI and SNI for their permanent support to the metallurgical process modeling group.

ISSN: 0012-7361 eISSN: 1989-1490 / DYNA March – April 2022 Vol.97 No 2 DOI: https://doi.org/10.6036/10206